Linking ocean and continental records of paleoclimate: determining accord and discord in the records

Frank R. Rack, Nathaniel W. Rutter, Andrew Bush, Dean Rokosh, and Zhongli Ding

Abstract: Climate forcing at Milankovitch and sub-Milankovitch frequencies are evaluated by linking climate proxy data from terrestrial and ocean records at two scales of temporal resolution: (1) relatively coarse resolution over the last 500 ka, and (2) higher resolution over the last 200 ka. We determine that climate proxy data from Hole 810C represent regional atmospheric and oceanic processes by comparison to core V21-146, both from the northwest Pacific Ocean. We then compare records that represent regional deposition from China and the western Pacific Ocean to focus on determining Milankovitch-type periodicities. Grain-size and magnetic susceptibility data from Hole 810C and Baoji, China are contrasted using a time-sensitive wavelet analysis. The analyses indicate a general correspondence to Milankovitch frequencies, although there is no specific frequency that dominates throughout the records. Additionally, the dominant 100 000 year frequency does not occur at the same time in the records. These factors suggest that differences in the physical mechanisms of deposition may influence the preserved apparent periodicities in these environments. Lastly, climate events over the last 200 000 years in marine and terrestrial records are correlated at a high resolution in the depth domain. The last interglacial–glacial boundary is consistently placed at the base of a cold period (C20) in the terrestrial and marine records. However, the cold period in the ocean data ($\delta^{18}O$) is very subdued relative to terrestrial records. Additionally, over the last 200 ka, periods of minimum insolation intensity do not correspond linearly to periods of maximum grain-size and ice volume variations revealed in the loess and ocean records, respectively. However, during the warm interstadials of the last two glaciations, peaks in insolation intensity compare favourably with the times of strongest pedogenic development in the continental records and minimum ice volume in the ocean records.

Résumé : Le forçage du climat à des fréquences Milankovitch et sous-Milankovitch est évalué en faisant un lien entre les données indirectes de sources terrestres et océaniques à deux échelles de résolution dans le temps : (1) une résolution relativement grossière pour les dernières 500 ka, et (2) une plus haute résolution pour les dernières 200 ka. Nous déterminons que les données indirectes du trou 810C représentent des procédés atmosphériques et océaniques régionaux par rapport à la carotte V21-146, les deux provenant du nord-ouest de l'océan Pacifique. Nous avons ensuite comparé les registres qui représentent une déposition régionale en provenance de la Chine et de l'ouest de l'océan Pacifique afin de se concentrer sur la détermination de fréquences de type Milankovitch. Des données granulométriques et de susceptibilité magnétique provenant du trou 810C et de Baoji, China sont mises en contraste au moyen d'une analyse temporelle des ondelettes. Les analyses indiquent une bonne correspondance générale aux fréquences de Milankovitch, bien qu'aucune fréquence spécifique ne domine à travers les registres. De plus, la fréquence principale de 100 000 ans ne se présente pas au même moment dans les registres. Ces facteurs suggèrent que des différences dans les mécanismes physiques de déposition peuvent influencer les périodicités apparentes préservées dans ces environnements. Finalement, dans le domaine de la profondeur, il y a corrélation à haute résolution entre les registres marins et terrestres des événements climatiques au cours des derniers 200 000 ans. La dernière limite glaciaire–interglaciaire est constamment placée à la base d'une période froide (C20) dans les registres marins et terrestres. Toutefois, la période froide dans les données océaniques ($\delta^{18}O$) est très atténuée par rapport aux registres terrestres. De plus, au cours des dernières 200 ka, des périodes d'intensité minimale d'insolation ne correspondent pas de façon linéaire aux périodes de granulométrie maximale et de variations des volumes de glace qui sont révélées respectivement dans les registres océaniques et de loess. Toutefois, au cours des réchauffements interstadiaires des deux dernières glaciations, des sommets dans l'intensité d'insolation se comparent favorablement avec les temps du plus fort développement pédogénique dans les registres continentaux et avec le volume minimal de glace dans les registres océaniques.

[Traduit par la Rédaction]

Received June 20, 1999. Accepted April 27, 2000.

F.R. Rack. Joint Oceanographic Institutions Inc., 1755 Massachusetts Ave. NW, Suite 800, Washington, DC 20036–2102, U.S.A.
N.W. Rutter,[1] A. Bush, and D. Rokosh. Department of Earth and Atmospheric Sciences, University of Alberta, Edmonton, AB T6G 2E3, Canada.
Z. Ding. Academica Sinica, P.O. Box 634, Beijing, China.

[1]Corresponding author (e-mail: nat.rutter@ualberta.ca).

Introduction

A fundamental requirement for understanding global climatic change is to compare and contrast proxy data from diverse environments such as terrestrial and deep sea environments. However, there are few studies that involve Quaternary ocean and terrestrial proxy climate records because of the difficulties involved in correlating and comparing these diverse environments. These difficulties include disparate proxy variables, poor stratigraphic control, and differences in thickness between the units. Rarely are the same proxy data available that would enable a direct comparison of the magnitude of climatic responses, or the forcing mechanisms involved in climate change. Further, there are no discernible global stratigraphic markers, such as ash layers or magnetic subchrons, to use as stratigraphic datum. Hence, correlations that link ocean and terrestrial environments are largely chronological, and assume linear sedimentation between control points such as magnetic boundaries or radiogenically dated samples.

To further our understanding of global climate change and address the inherent difficulties in ocean-terrestrial research we present a comparison of oceanic and terrestrial proxy data at two scales of temporal resolution: (1) relatively coarse resolution over the last 500 ka, and (2) high resolution over the last 200 ka. By analyzing the data at two different temporal resolutions we can examine climate forcing in terrestrial and oceanic environments at Milankovitch and sub-Milankovitch frequencies. We have selected coarse resolution records that meet a relatively rigorous set of criteria: (1) the ocean and terrestrial proxy climate variables must be alike, (2) the sites selected in each environment must comprise relatively thick strata, with sample strategies that enable us to compare records with reasonably similar temporal resolutions, and (3) we use ocean and terrestrial records that are interpreted, in part, as recording glacial to interglacial variations in eolian processes.

In our coarse resolution analysis, we provide evidence of eolian sedimentation from Ocean Drilling Program (ODP) Hole 810C (latitude 32°25.40′; longitude 157°50.44′) in the northwest Pacific Ocean. Data from this site contains, in our judgement, a very good record of terrigenous sedimentation and have never been published. Data from 810C are then compared to V21-146 (latitude 37°41.00′; longitude 163°02.00′), also from the northwest Pacific Ocean, to establish that these records reflect regional eolian sedimentation. We then investigate temporal variability of Milankovitch-type periodicity in the ocean and terrestrial data by performing wavelet analyses on grain-size and magnetic susceptibility variations from Hole 810C as well as from Baoji, China. To our knowledge, this is the first time that a wavelet analysis has been performed on multiple (and similar) records of proxy data from marine and terrestrial environments. The Baoji site was selected because it is one of the most studied and has the most complete records of alternating loess and paleosols in the Loess Plateau, China. There appears to be some common ground between the two sites, in that the eolian material in the western Pacific Ocean has been interpreted as sourced from the arid regions of China (Rea 1994). However, we cannot be certain at this time that the eolian sediment from Hole 810C is sourced from the Chinese deserts. In this respect our evaluation is preliminary.

In the high-resolution comparison we correlate records from the Loess Plateau, China to ocean $\delta^{18}O$ records over the last 200 000 years. We do not use Hole 810C for this analysis because of the coarse sample resolution, and there are some indications of bioturbation in the upper few meters of the ocean record (Storms et al. 1991) Instead we have chosen records from both the Indian and Pacific oceans because of the high-resolution sampling strategy, and to show that our ocean-terrestrial correlations represent a hemispherical paleoclimate connection. We have also chosen to use data from Wupu and Yanchang in the Loess Plateau, rather than the Baoji site. The Wupu and Yanchang records exhibit thicker units over the last 200 000 years than Baoji, and are more suitable for a high resolution comparison. We construct an ocean-terrestrial stratigraphic template that should result in a more consistent determination of high resolution climate boundaries in these diverse environments and, with improvements in the resolution of absolute dating, lead to more precise interpretations of global climate history. We use the template to examine sub-Milankovitch climate forcing by comparing continental loess records with ocean ice volume data and the insolation record of Berger and Loutre (1991).

Coarse resolution analysis

In the coarse resolution analysis, our objectives are threefold: (1) examine the terrigenous data from Hole 810C and determine if the record represents glacial to interglacial variations in eolian sedimentation; (2) compare the 810C data to the records from nearby V21-146 (Fig. 1), and determine if these data represent regional records of eolian sedimentation, and (3) perform a wavelet analysis on grain-size and magnetic susceptibility data from Hole 810C and the well-known Baoji section to determine areas of accord and discord with respect to the presence of Milankovitch-type frequencies.

Sedimentary records from aseismic rises of the northwest Pacific Ocean have focussed on studying dust distribution in marine sediments through time mainly because they (1) are generally above the calcium carbonate compensation depth (CCD) in this part of the ocean (Farrell and Prell 1991; Haug et al. 1995), (2) are located south of ice-rafted sediments deposited during glacial intervals (Krissek et al. 1985; Krissek 1995), and (3) lie far from riverine and continental shelf sources of hemipelagic sediment (Olivarez et al. 1991; Nakai et al. 1993; Rea 1994; Rea et al. 1985; Weber et al. 1996).

It is generally accepted that Cenozoic fluctuations in (terrigenous) mineral mass accumulation rates in the northwest Pacific have resulted from changes in the aridity of source regions (e.g., the Loess Plateau, China), while changes in the median grain-size of the mineral particles have resulted from changes in the energy or strength of atmospheric winds (Leinen and Heath 1981; Rea and Janecek 1981, 1982; Janecek and Rea 1983, 1985; Rea 1994). Piston core V21-146, which was collected in 3968 m of water on the northern part of Shatsky Rise (Fig. 1; Hovan et al. 1989, 1991), provides the best-available record of fine-grained

Fig. 1. Map showing the location of ODP Hole 810C and piston core V21–146.

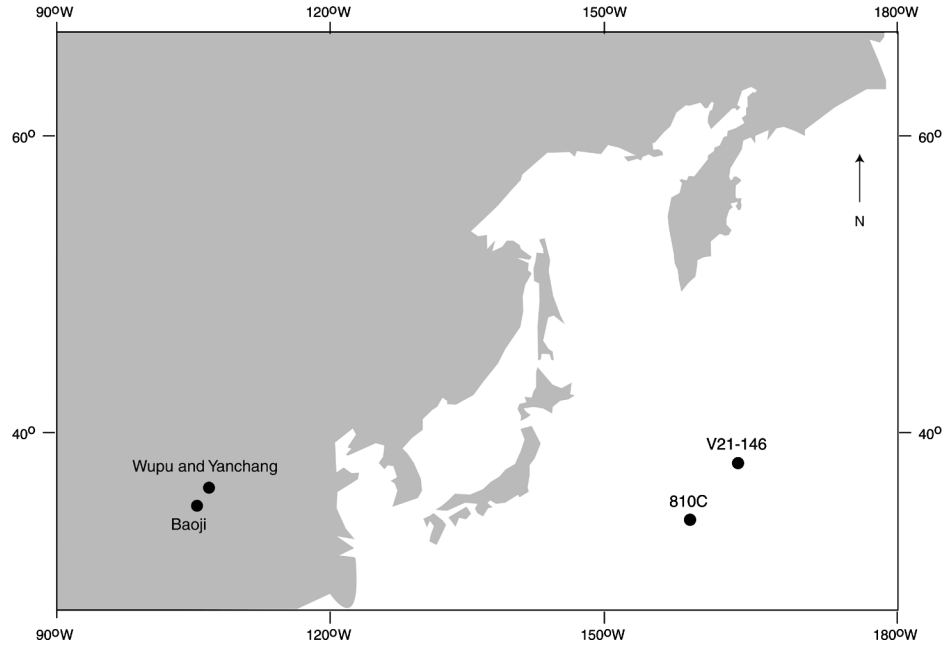

Fig. 2. Location of the Loess Plateau, China and sites mentioned in the text.

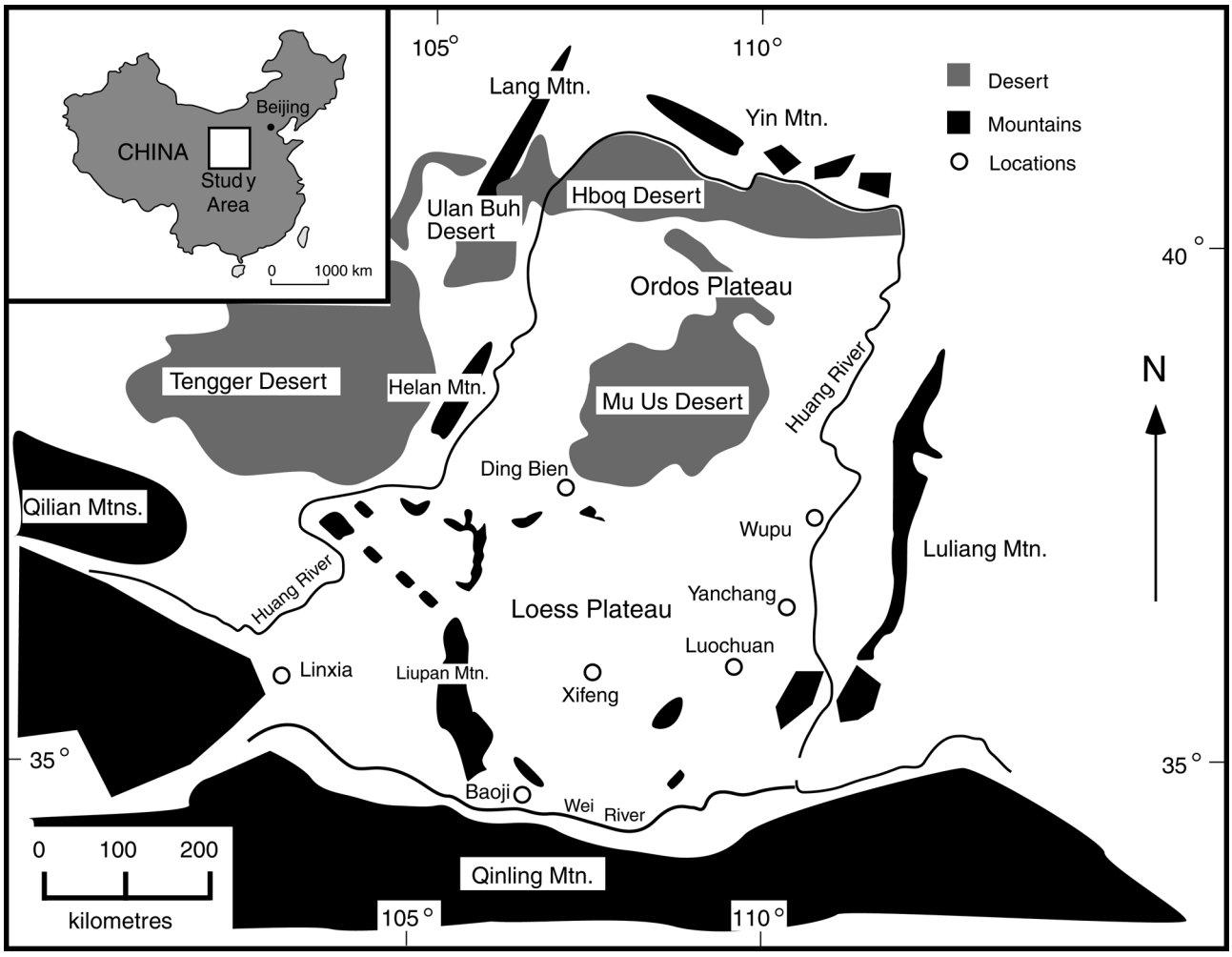

Fig. 3. Summary of Hole 810C to a core depth of 10 m, southern Shatsky Rise, showing the lithologic, paleomagnetic, and physical properties of the sediment recovered in the upper 10 m.

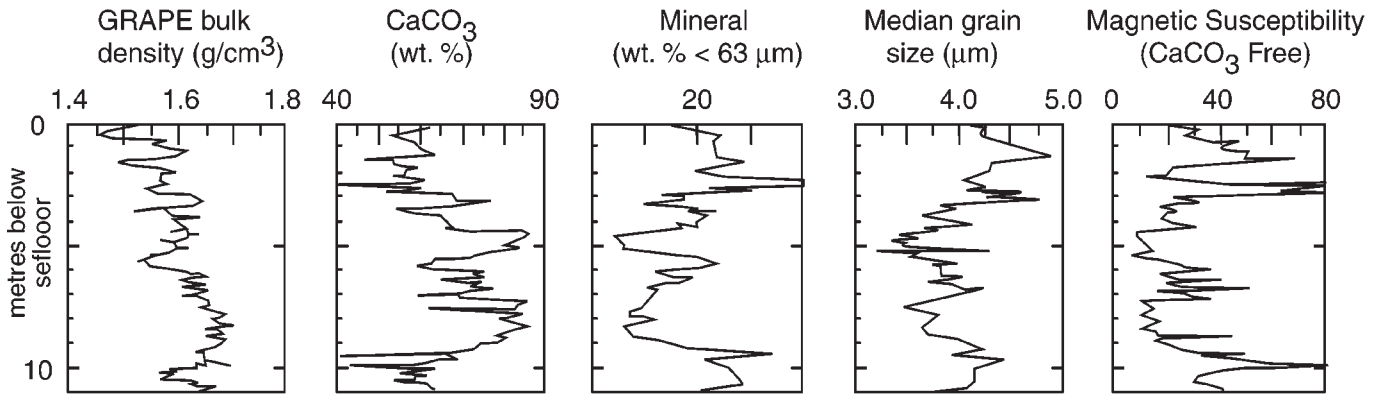

terrigenous mineral flux in the northwest Pacific Ocean for the past ~500 000 years. Studies of this core have allowed a direct comparison of mineral dust transported to the Pacific Ocean and magnetic susceptibility records of continental loess deposits from Xifeng, China (Fig. 2; Hovan et al. 1989, 1991; Kukla et al. 1990).

The interpretation of the eolian nature of the mineral record from piston core V21-146 (see Rea 1994) may be questioned for three reasons. (1) The core is located below the mean flow path of the Kuroshio Current Extension at the northern end of Shatsky Rise. This is a region of high eddy kinetic energy (Joyce 1987; Schmitz et al. 1987; Koblinsky et al. 1989; Chao 1994; Hurlburt et al. 1996) which may be affected by erosion or re-sedimentation (Jacobi and Hayes 1989). (2) Volcanic ash is present in the core. The effect of small quantities of dispersed volcanic ash and hemipelagic sediment on the median mineral grain size of samples from core V21-146 is poorly understood. (3) To our knowledge there is a lack of published grain-size distributions from this site (excluding surface samples), and only median grain-size data are available.

Ocean Drilling Program Hole 810C, located in 2623 m of water on the southern portion of Shatsky Rise (Fig. 1), yields evidence of cyclic changes in the fine-grained mineral fraction of the bulk sediment and carbonate content, with relatively long periods of deposition during the last 0.5 Ma. Siliceous microfossils are prevalent in the upper 4.2 m, where cut and fill structures are evident (Storms et al. 1991) indicating current winnowing and erosion. Several discrete ash layers found within the sequence may be correlated to ash layers identified at other northwest Pacific drill sites (Natland 1993) and ultimately provide insight into wind strength fluctuations independent of continental aridity assumptions, such as those typically used in eolian studies of continental dust (Rea 1994).

Changes in the grain-size distribution of the fine-grained mineral component in over 150 sediment samples covering the last 0.5 Ma from Hole 810C are used to (1) establish the eolian character of this site; (2) determine the influence of episodic volcanic sedimentary input and (or) the interaction of ocean currents with the sediment preserved on Shatsky Rise; and (3) evaluate possible paleoceanographic and paleoclimatic variations. Terrigenous mineral data from both Hole 810C and piston core V21-146 are used to evaluate latitudinal changes in the flux of terrigenous minerals and mineral grain-size across 6° of latitude between 38°N and 32°N. To establish age control for these fluctuations, we present an integrated stratigraphy based on an interpretation of (1) magnetic polarity reversals, (2) semi-quantitative nannofossil biostratigraphy, and (3) correlations to the SPECMAP oxygen isotope timescale (Imbrie et al. 1984) through comparisons between the carbonate records from Hole 810C and piston core V21-146.

Methods

ODP Hole 810C provides a record of the mass accumulation of biogenic and mineral sediment (Fig. 3). Carbonate content was determined from measurements of inorganic carbon as described in Rack et al. (1993). The mineral component of the bulk sediment, including contributions from both terrigenous and volcanic sources, was isolated by a series of selective chemical extractions to remove calcium carbonate, opaline silica, iron and manganese oxides, hydroxides, and zeolites (Rea and Janecek 1981; Clemens and Prell 1990). The material passing through a 63 μm sieve after the completion of the extraction procedure was weighed to determine the weight percentage of the fine-grained mineral fraction (<63 μm) in the bulk sample (Rack et al. 1995). A Coulter LS130 laser particle size analyzer with a fluid module and a PIDS (Polarization Intensity Differential Scattering) assembly was used to determine the particle size distribution of chemically extracted fine-grained mineral samples using a Fraunhofer-theory optical model (Coulter 1992). For most intervals, 1 out of 5 carbonate samples was used to conduct mineral extraction and grain-size analyses due to financial limitations.

Small amounts of ash can significantly influence the grain-size distribution (Rea 1994; Rea and Hovan 1995) in the coarse silt to fine sand range, due to their irregular shape and vesicularity (Natland 1993), and influence calculations of the relative degree of sorting. There are many additional issues related to the choice of methods for sample preparation and the instrumentation used in grain-size analyses, but these are well covered by other authors (Konert and Vandenberghe 1997; McCave and Syvitski 1991; McCave et al. 1995).

Additional published data from Hole 810C include (1) non-destructive measurements of whole-core magnetic

Fig. 4. Summary of mass sediment accumulation rates for core V21–146 (dotted line) and Hole 810C (solid line) plotted on the V21-146 time scale. LSR, linear sedimentation rate; DBD, dry bulk density; MAR, mass accumulation rate; CAR, carbonate accumulation rate; NCAR, noncarbonate accumulation rate; and Mineral MAR, mineral mass accumulation rate.

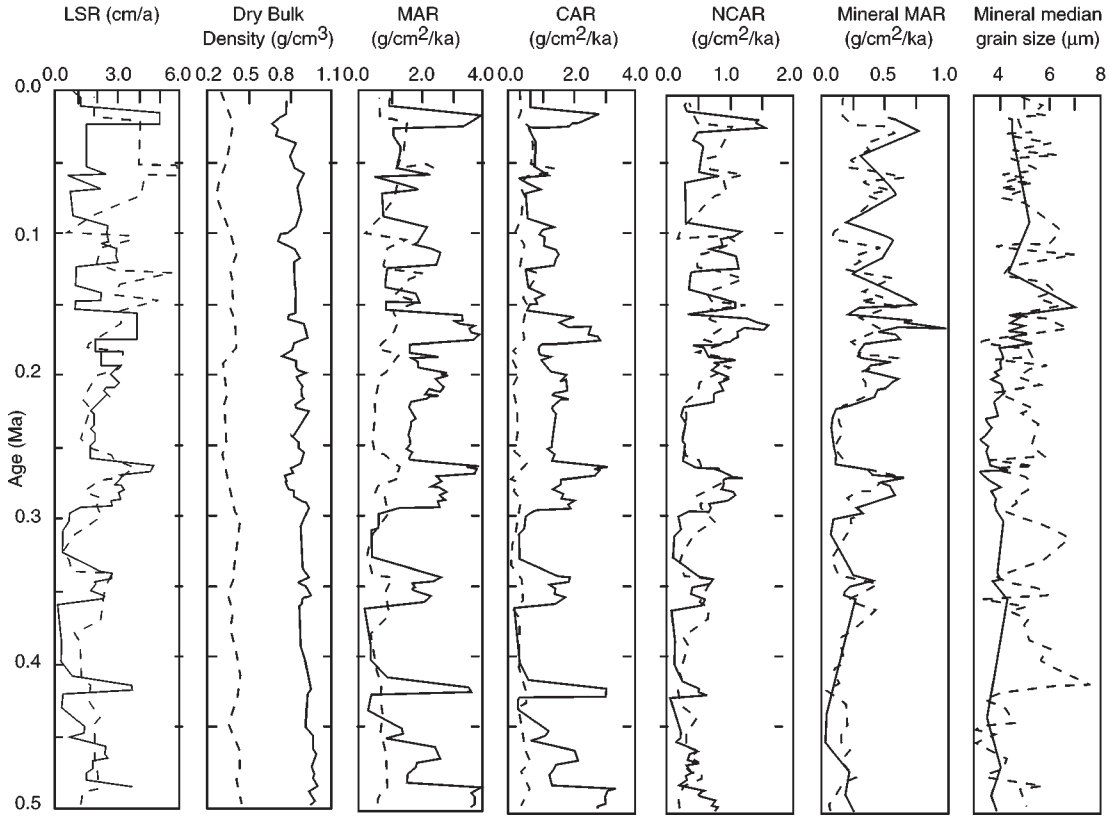

susceptibility and gamma density (GRAPE and GRA both refer to measurements of gamma ray attenuation) using sensors mounted on the ODP multi-sensor track (Storms et al. 1991), (2) measurements of paleomagnetism and magnetic stratigraphy (Sager et al. 1993), and (3) semi-quantitative calcareous nannofossil and foraminifer abundance (Premoli Silva et al. 1993). We assume synchronous ages between the nannofossil datums identified in Hole 810C and those defined for the equatorial Pacific (Raffi et al. 1993; Raffi and Flores 1995; Shackleton et al. 1995).

Sediment mass accumulation rates (MAR = $g \cdot cm^{-2} \cdot ka^{-1}$; Fig. 4) were calculated as the product of the linear sedimentation rate (LSR = $cm \cdot ka^{-1}$) and the dry bulk density ($g \cdot cm^{-3}$); accumulation rates of carbonate and mineral components of the bulk sediment were obtained by multiplying the bulk MAR and the fractional proportion of each component. The dry bulk density of each sample was determined using a regression of gamma density on discrete volumetric measurements of dry bulk density. The dry bulk density of the sediment from Hole 810C is about 2 to 2.5 times higher than the dry bulk density values determined for core V21-146, which were estimated from the weight percentage of dry salt in each sample (Hovan et al. 1991).

The past 500 ka: a comparison between core V21-146 and Hole 810C

The upper 10 m of sediment in Hole 810C are equivalent to the past 0.5 Ma, based on a detailed correlation of carbonate fluctuations between core V21-146 and Hole 810C (Fig. 5), a distance of approximately 500 km north–south. The carbonate and noncarbonate curves match well throughout the records, with Hole 810C typically showing 30–40% higher carbonate values. This may be due to the water depth differences, and therefore carbonate preservation, between these two sites. The mineral fraction (<63 μm) in both records also exhibit a good correspondence in the zones where the sample resolution in Hole 810C are highest (e.g., 150–300 ka).

The carbonate mass accumulation is up to four times higher in Hole 810C than for core V21-146 within correlated carbonate intervals (Fig. 4). The mineral mass accumulation rates are nearly identical at both locations, suggesting that the mineral flux changes were relatively coherent across 6° of latitude in this area. The differences in dry bulk density between these two sites may be interpreted as differences in the relative abundance of biosiliceous and calcareous microfossil skeletons and (or) changes in texture and packing of the sediment. This effect may be strengthened by increased northward carbonate dissolution and (or) the water depth difference (i.e., 1345 m) between core V21-146 and Hole 810C, which places core V21-146 just above the calcium compensation depth in this area of the Pacific. There is little information available on the preservation of microfossils from core V21-146, but we suspect that they are more poorly preserved than those from Hole 810C given the greater water depth.

The median mineral grain size is generally larger and more variable (Figs. 4, 5) in core V21-146 (to the north)

Fig. 5. Comparison between Hole 810C and piston core V21-146 based on the correlation of calcium carbonate records from the two sites (solid lines, Hole 810C; dotted lines, core V21-146), and plotted on the core V21-146 timescale (left, modified from Hovan et al. 1991), which is coherent with the ages assigned to SPECMAP marine oxygen isotope stages (Imbrie et al. 1984).

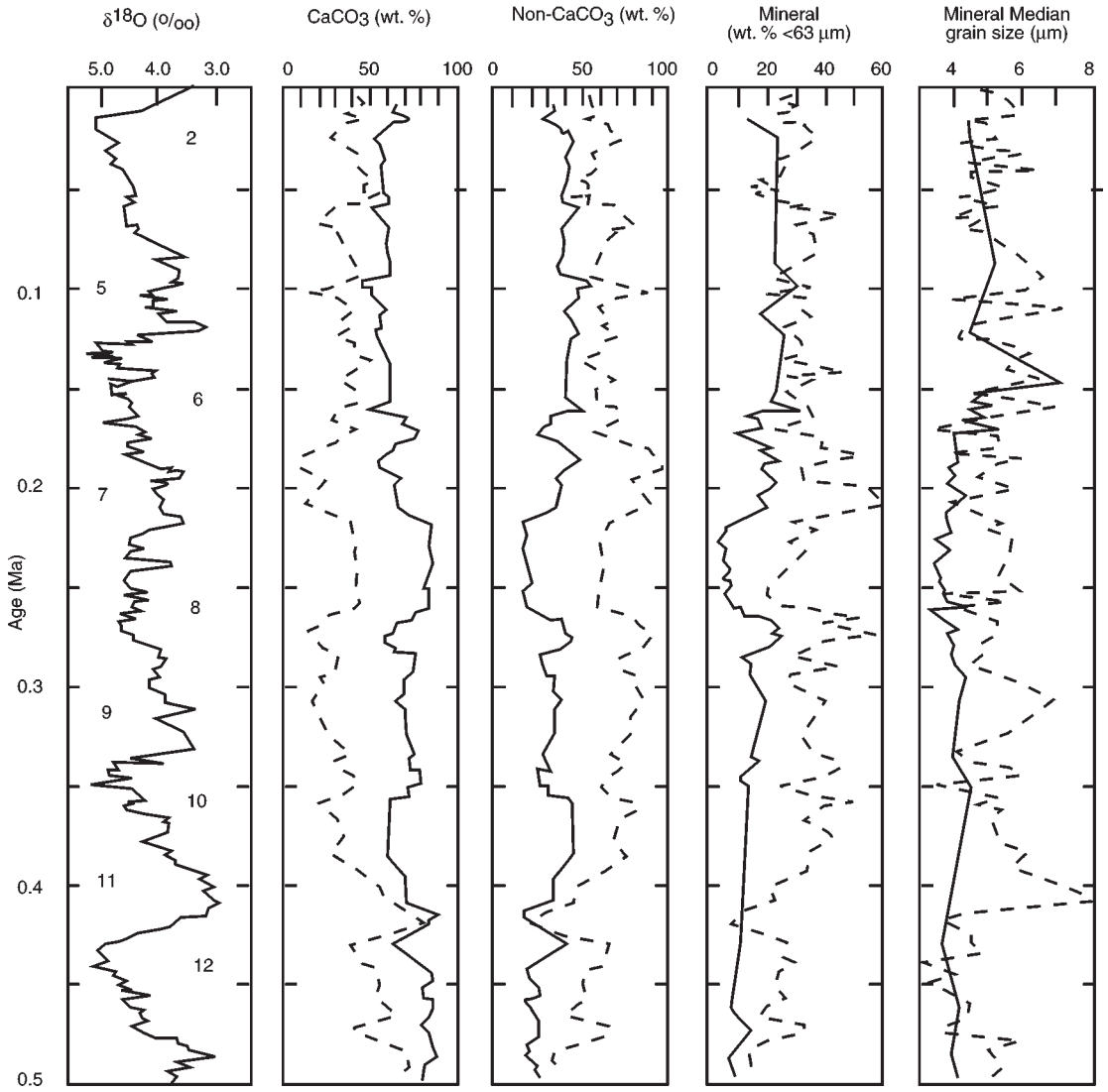

than in representative intervals from Hole 810C. However, slightly different methods of analysis and sample preparation were used to determine the median grain size from core samples. Hovan et al. (1989, 1991) passed their samples though a 38 μm diameter sieve and set the Coulter Counter to measure the 1–30 μm fraction. Note that the <1 μm fraction was not measured in core V21-146, while that fraction is included in the Hole 810C data. To examine the affect of the different method of analysis on median grain size, we calculated both the median grain-size of the entire population in Hole 810C and the median size of only those grains below 31 μm. We obtained similar results in both sets of data, indicating that the different methods may not have a significant affect on the derivation of median grain size. The average of the median mineral grain size in the upper 10 m (~500 ka) of Hole 810C is about 3.8 ± 0.4 μm, with significant coarsening to about 5–7 μm during inferred glacial stages (Figs. 5, 6).

A slightly higher ash content in the fine-grained sediment of core V21-146 relative to the corresponding intervals from Hole 810C could be responsible for the larger median grain size. Alternatively, sediment from core V21-146 may exhibit a slightly more hemipelagic character than Hole 810C sediment. Shatsky Rise lies between the hemipelagic and eolian zones described by Rea and Hovan (1995) who used core top samples from all across the North Pacific to construct these zones.

The particle size distribution of selected samples from Hole 810C is shown for the interval 0–8.05 m (Figs. 6A, 6B, 6C, 6D). The histograms show that the samples are poorly sorted according to the definition of Folk (1974). This poor sorting may support either of the previous two explanations for the presence of silt size modes, both of which may be linked to changes in the vigor of atmospheric and (or) ocean circulation. We do not have data from V21-146 to make a comparison of sorting. Pumice grains, ash layers, and intervals of dispersed ash have been identified in Hole 810C by Natland (1993). We can identify six of these ashes by their characteristic grain-size distribution (Fig. 6E). The coarse silt mode and skewed distribution of the ash samples are

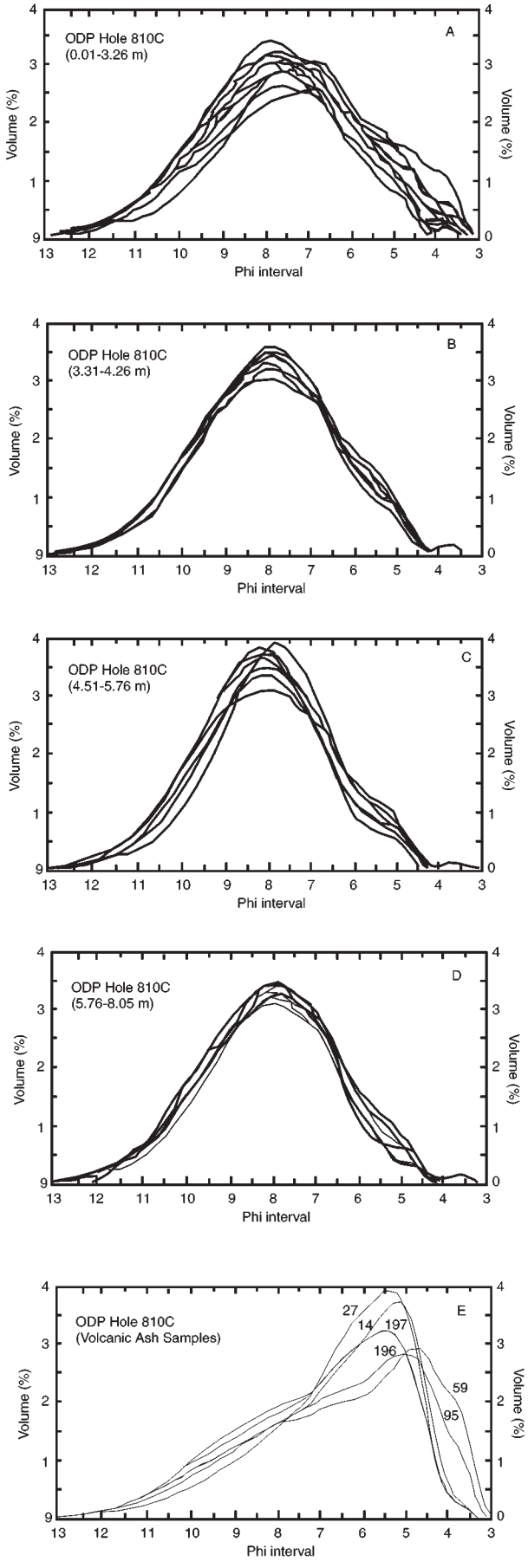

Fig. 6. (A to D) Histograms of the grain-size distribution from the upper 8.05 m of Hole 810C. Each plot shows the resulting particle size distributions from 20 individual samples. (E) Grain-size distribution of volcanic ash samples showing a skewed particle size distribution and a medium to coarse silt mode. Phi 4 = 62.5 μm; phi 8 = 3.9 μm; phi 12 = 0.24 μm.

similar to the secondary modes seen in many of the other sample grain-size distributions, suggesting the presence of ash in these samples. Several large tephra eruptions are known to have occurred in southern Japan during the late Quaternary. These include, the 6 300 BP Kikai–Akahoya (K–Ah) tephra, the 22 000–25 000 BP Aira–Tanzawa (AT) tephra, the 70 000–90 000 BP Aso–4 tephra, and the 75 000–95 000 BP Kikai–Tozurahara (K–Tz) tephra (Furuta et al. 1986; Machida and Arai 1976, 1978, 1983, 1988). Without microscopic visual observations, or geochemical partitioning of end members in these samples, an assumed a mixture of ash and dust is the most likely interpretation of our results, given the proximity of volcanic arcs located to the west and northwest of Shatsky Rise.

Wavelet analysis

Information on temporal variability in the records is extracted through a wavelet analysis. This analysis is similar in principal to a Fourier analysis and can extract periodicity information from a time series. Unlike Fourier analysis, however, it reveals periodicity as a function of time. This added feature arises from the localized nature of the Morlet wavelet; in contrast, the sine and cosine functions used in Fourier analysis are not localized and therefore cannot be used to determine when a particular periodicity occurs in a given time series. In the following figures, two sloping lines have been plotted on the wavelet power spectrum. The analysis is valid between these two lines; darker shades indicate more power. To perform the analyses, irregularly spaced data from the last 500 ka are interpolated to an evenly spaced time series through a cubic spline interpolation.

Wavelet analyses of the marine susceptibility and grain-size data (Figs. 7, 8) indicate significant power at a period of approximately 35 ka between 100–250 ka. The ~120 ka maximum in the susceptibility data is not seen in the grain-size record; rather, two maxima at ~160 ka and ~64 ka are indicated in the grain-size data. A relatively strong ~10 ka signal at approximately 220 ka is apparent in the susceptibility data and, to a lesser extent, in the grain-size data.

The analysis of the last 500 ka of the Baoji susceptibility data (Fig. 9) indicates a ~100 ka peak over the last 250 000 years. Prior to this a ~90 ka period is dominant. There is also significant power at period of ~41 ka throughout much of the record. The Baoji grain-size data indicate power at a ~120 ka period between 200 ka and 500 ka (Fig. 10). The dominant signal, however, is a ~15 ka period that occurs throughout most of the record.

The periodicities in these four records demonstrate a complex temporal structure. Some records indicate strong power at a particular frequency while others do not. The Baoji grain-size data, for example, demonstrates virtually no signal at the ~41 ka period, in contrast to the susceptibility data where power at this period is prominent. The marine grain-size data indicate a strong 160 ka period from about 150–

Fig. 7. (A) Time series of actual magnetic susceptibility data (solid points) and interpolated data (open points) from Hole 810C in the Northwestern Pacific Ocean, (B) Wavelet analysis power spectrum. Darker shading indicates more power at that period.

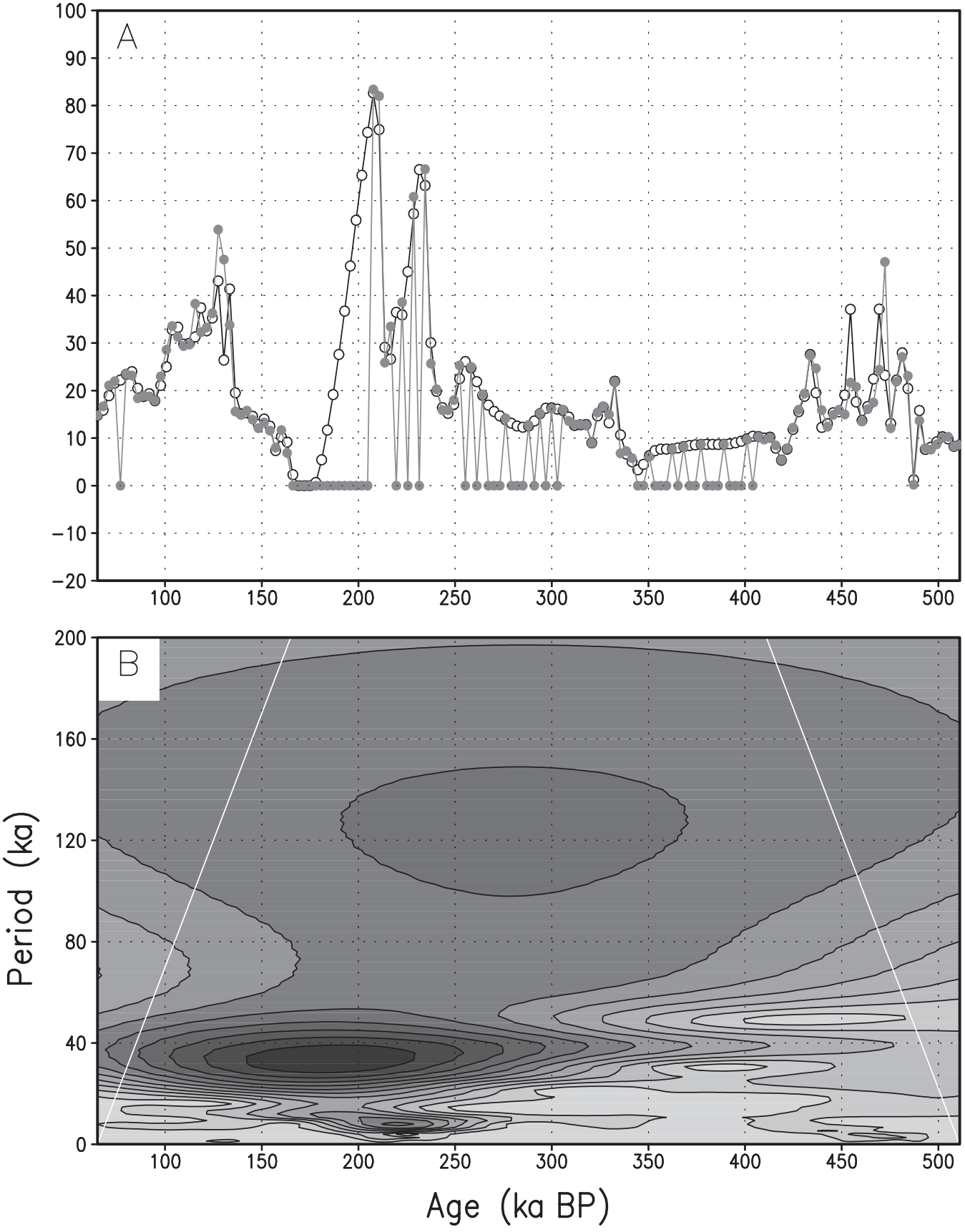

Fig. 8. (A) Time series of actual grain-size data (solid points) and interpolated data (open points) from Hole 810C in the Northwestern Pacific Ocean. (B) Wavelet analysis power spectrum from Hole 810C. Darker shading indicates more power at that period.

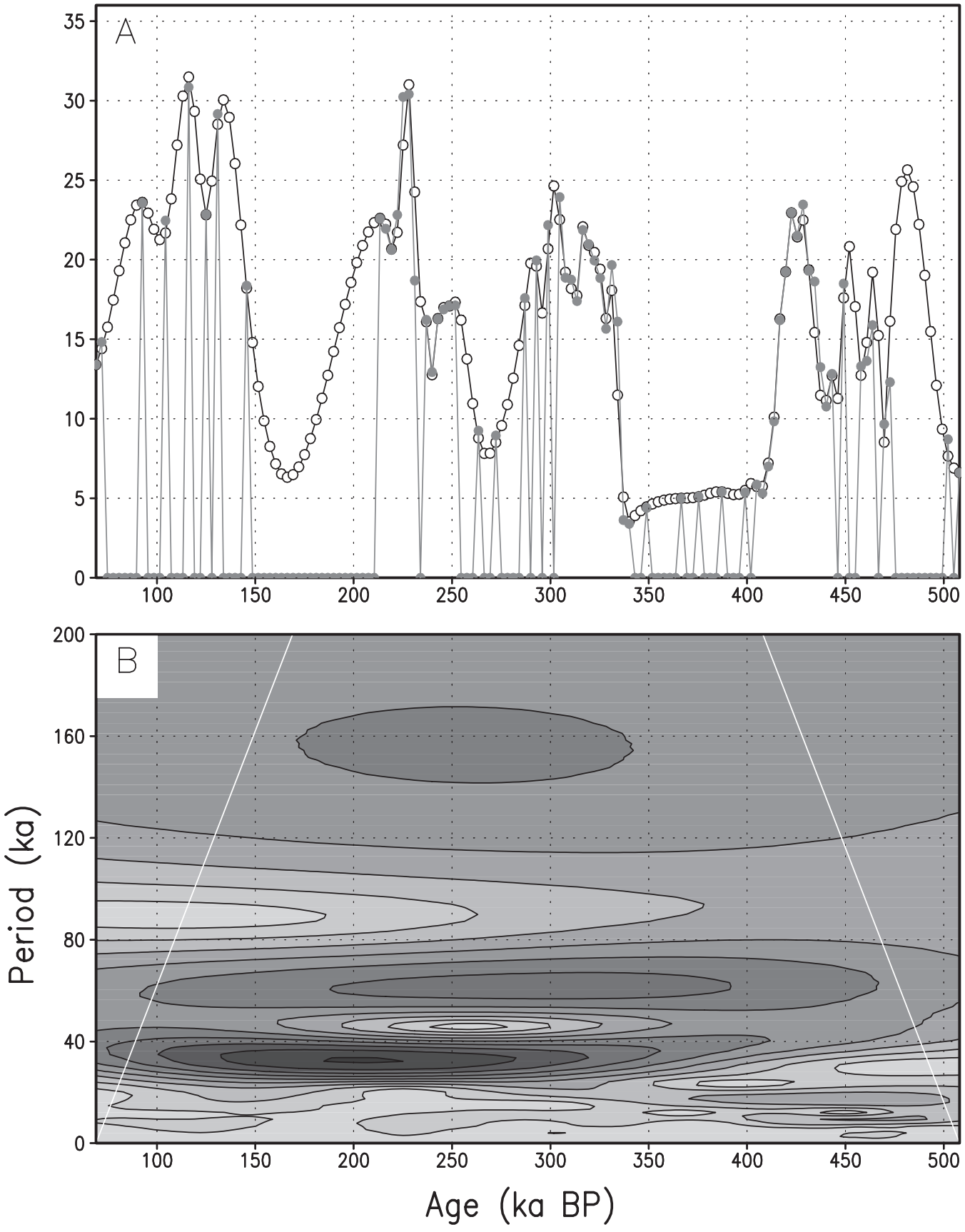

Fig. 9. (A) Time series of actual magnetic susceptibility data (solid points) and interpolated data (open points) from Baoji in the Loess Plateau, China. (B) Wavelet analysis power spectrum from Baoji. Darker shading indicates more power at that period.

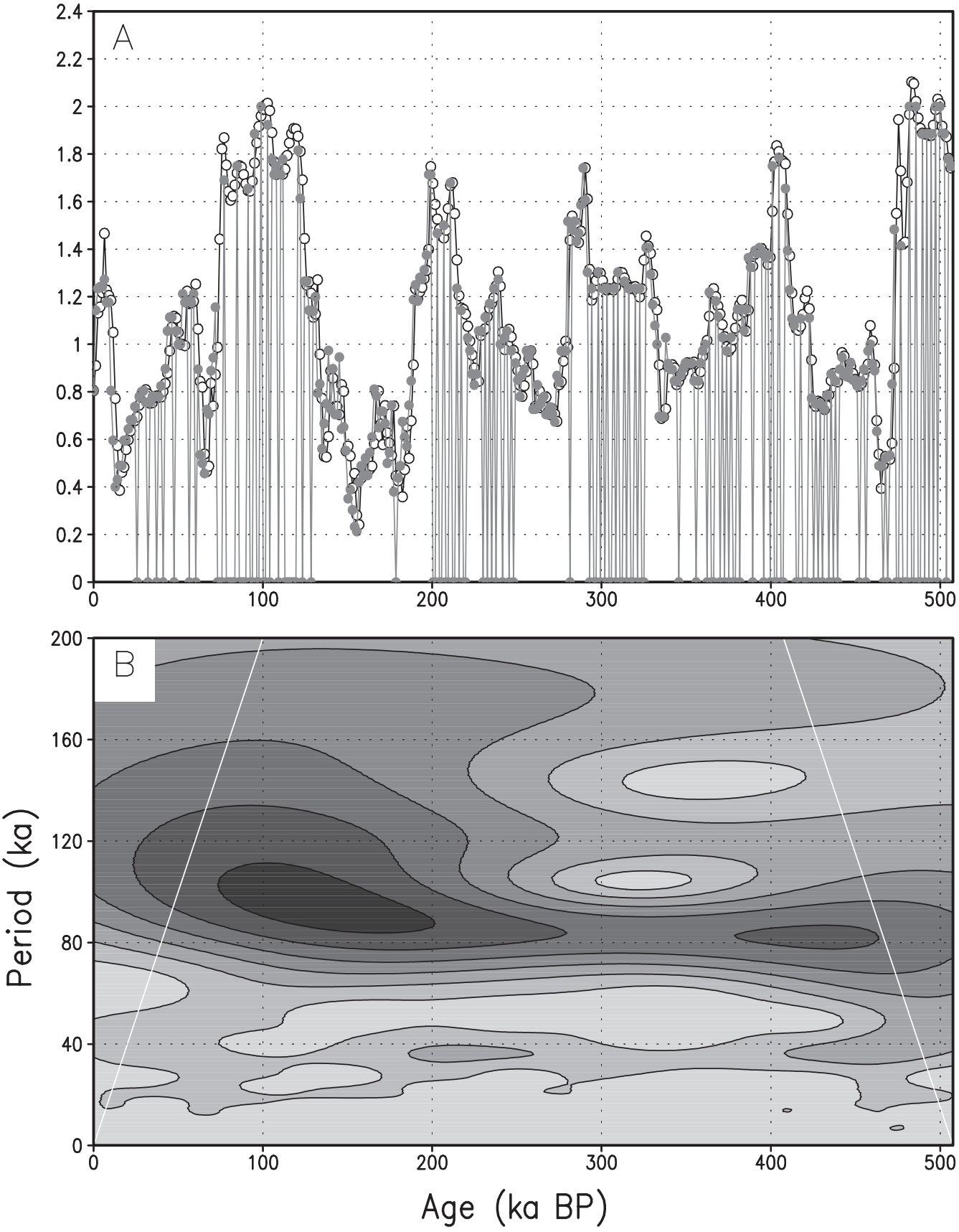

Fig. 10. (A) Time series of actual grain-size data (solid points) and interpolated data (open points) from Baoji in the Loess Plateau, China. (B) Wavelet analysis power spectrum from Baoji. Darker shading indicates more power at that period.

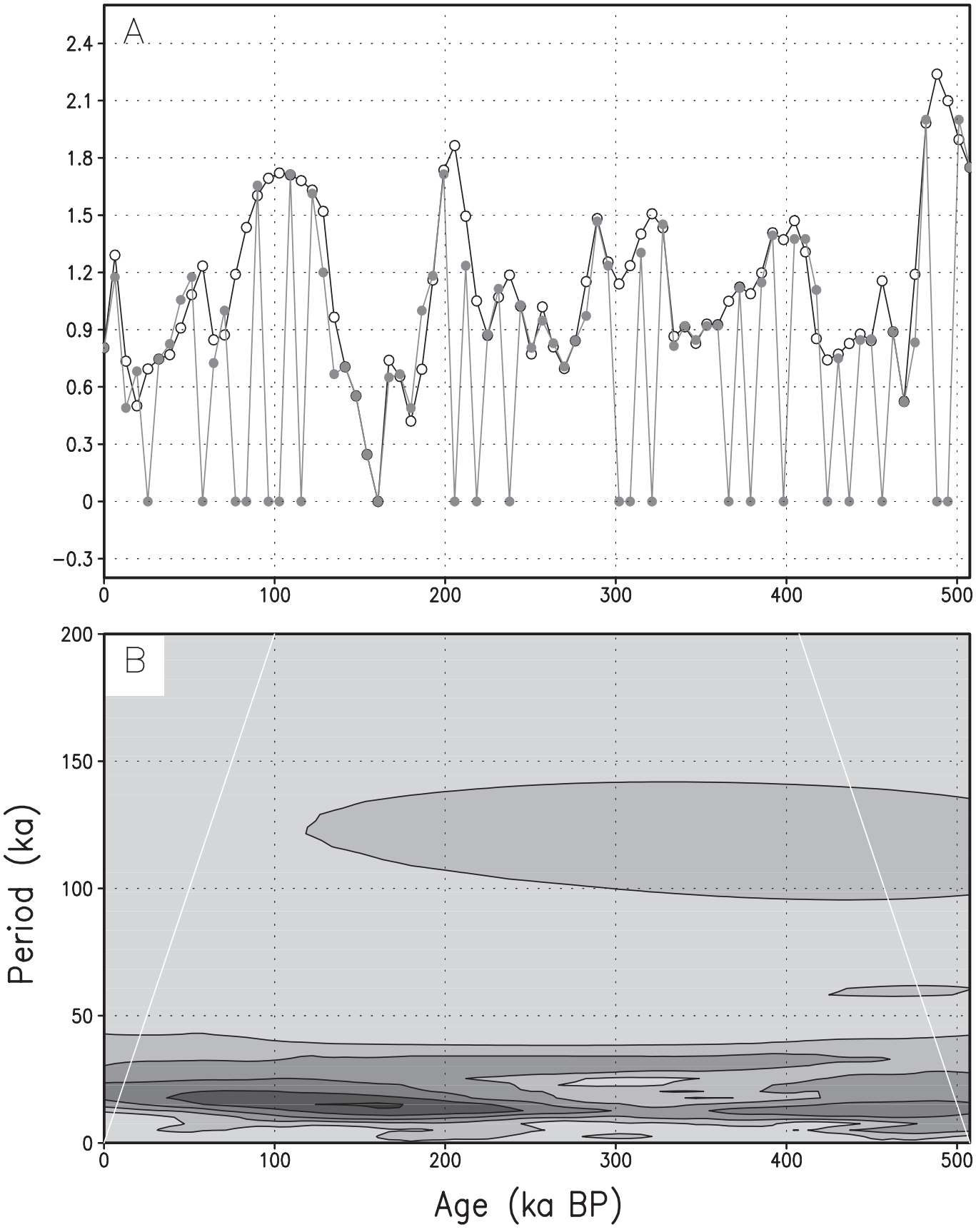

350 ka. The marine susceptibility and the terrestrial grain-size both indicate strong 120 ka signals from about 200–350 ka and 100–450 ka, respectively.

Periodicities approaching the Earth's orbital parameters appear most clearly in the terrestrial susceptibility data (Fig. 9), but they are nevertheless only a part of the entire spectrum. A visual inspection of the Baoji susceptibility time series (Fig. 9A) shows that there are no time intervals where the variability is strictly periodic, so the 100 ka signal is in some sense a "best fit" rather than an indication of orbital forcing. The same can be said for the ~41 ka signal in the record.

High resolution records

Ocean–terrestrial correlations are normally done in the time domain because of the large differences in thickness between these environments. The time scale is, in part, determined by assuming linear sedimentation between control points (Imbrie et al. 1984). In contrast, our comparison of terrestrial and oceanic records use depth scales, similar to Prell et al. 1986, to avoid the assumption of linear sedimentation between temporal control points. However, the data are set within a temporal framework in a manner similar to Imbrie et al. (1984). Our strategy is to search for warm periods within a glacial interval that have a long enough time span, and show sufficient warming, to be recognizable within the resolution of the data in all environments. In this manner the warm periods are regarded as high resolution climostratigraphic markers, or control points.

We have chosen to correlate high-resolution records that are not only derived from diverse environments, but that also span a large latitude of the northern hemisphere. In this manner, areas of accord and disaccord between the records may be become apparent. We first compare our mid-latitude loess records with the relatively high-latitude GISP2 Greenland ice core. The Greenland ice cores are a climate proxy standard that have been used to compare interpretations from other proxy data. We use the ice-core data to validate the climatic interpretations from mid-latitude loess records. After establishing that the loess and ice-core records reflect hemispherical climate change, we then compare loess records to high resolution tropical ocean proxy data to examine the consistency of glacial–interglacial boundaries between these environments, and further our understanding of climate forcing relationships.

Methods

Grain size and magnetic susceptibility were determined on loess and paleosol samples from Wupu and Yanchang in the central Loess Plateau (Fig. 2). Samples were taken every 10 cm loess beds and 5 cm in paleosols. Since paleosols are thinner than loess beds, the smaller sample interval in S1 reflects an increase in the temporal resolution within the paleosol. Bulk magnetic susceptibility and grain size was determined on each sample. Grain-size analysis was performed on a PRO-700 SK Laser Micron Sizer. An analysis of 20 replicate samples indicated a precision of 3.5%. Organic material, pedogenic iron, and carbonate were removed prior to grain-size analyses. Bulk magnetic susceptibility was determined using a Bartington MS II susceptibility meter. Susceptibility values represent one reading on an approximately 50 g bagged sample. The values are presented as carbonate-free by calibrating each sample to the amount of carbonate present. The formula A2 = A1(100/100 wt.% C) was used to calibrate the samples, where A1 and A2 are the measured and resultant magnetic susceptibility, respectively, and C is the wt.% carbonate. Paleosols in the Loess Plateau have a high susceptibility and are largely carbonate free (Liu et al. 1985), so the calibration results in little change in the paleosols. Our loess samples contain a maximum of 10–15 wt.% carbonate; however, loess susceptibility is low in the northern Loess Plateau, relative to soils (Liu et al. 1985), so the magnitude of the change is relatively small.

China and Greenland

Grain-size and magnetic susceptibility variations from the Loess Plateau are proxies for variations in winter and summer monsoon intensity, respectively, (Liu et al. 1985). The resolution of loess-paleosol records from the Chinese Loess Plateau is much higher during glacial periods than interglacial periods (Liu et al. 1985); hence we concentrate our efforts on glacial periods. A temporal framework for the last 200 000 years (Figs. 11, 12) has been determined by Berger and Loutre (1991), who noted the presence of positive (warm) and negative (cold) shifts relative to the AD 1950 insolation value at 65°N latitude.

Chinese loess-paleosol records have previously been compared to Greenland ice cores (Porter and An 1995, Chen et al. 1997, Rutter et al. 1997), so we can contrast our interpretations with previous work and determine the regional (or local) nature of proxy climate signals from the Loess Plateau. Firstly, we compare loess records from China (Fig. 11), during MIS 2–4, with the GISP2 2 m $\delta^{18}O$ profile (Grootes et al. 1993; Meese et al. 1994; Stuiver et al. 1995) and establish a climostratigraphic framework using the Emiliani (1955) concept of oxygen isotope stages, and the Berger and Loutre (1991) insolation record. Although climostratigraphy does not necessarily reflect chronostratigraphy (North American Stratigraphic Code 1983), we use major glacial–interglacial boundaries (e.g., MIS 6–5 and 2–1) as temporal control points, in a manner similar to Imbrie et al. (1984). It is important in this comparison that the resolution of the records are reasonably similar. The resolution of the L1 loess is about 575 years per sample, while the resolution of the GISP2 2 m profile is about 30–40 years at the MIS 1–2 boundary and increases to about 300 years at the MIS 5–4 boundary. Although the resolutions are not the same, this is the best data available.

Loess L1 at Wupu and Yanchang (Fig. 11) is subdivided from bottom to top into L1–5 through L1–1, representing three loess intervals (L1–5, L1–3, and L1–1) and two weakly developed paleosols (L1–4, L1–2). This subdivision is regionally consistent in the central Loess Plateau (Sun and Ding 1998). A correlation between oceanic $\delta^{18}O$ and loess-paleosol records (Liu et al. 1985; Kukla 1987; Ding et al. 1991) suggests that marine oxygen isotope stages (MIS) 2, 4 and 6 correspond to loess subhorizons L1–1, L1–5, and L2 respectively, MIS 3 corresponds to L1–2, L1–3, and L–1–4; and Paleosols S0, S1, and S2 correspond to MIS 1, 5, and 7, respectively. In this report the nomenclature system utilized by McManus et al. (1994; see also Johnsen et al. 1992) is

Fig. 11. Comparison of proxy climate records from China and Greenland with the insolation record of Berger and Loutre (1991). The Berger and Loutre (1991) insolation values are calculated relative to the AD 1950 value of 427 W·m^{-2}.

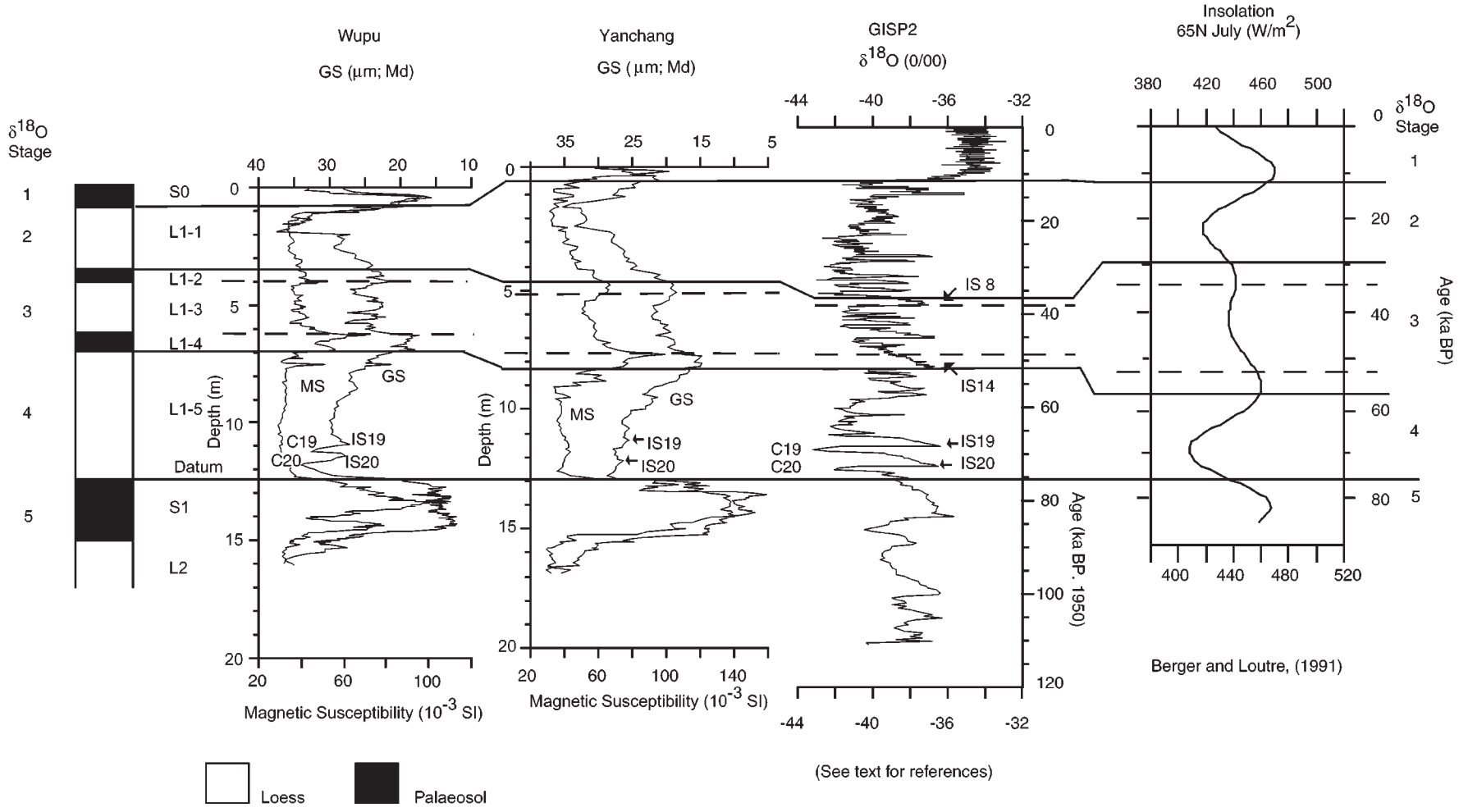

Fig. 12. Comparison of loess-paleosol stratigraphy with $\delta^{18}O$ records from the Indian and Pacific oceans. The Berger and Loutre (1991) insolation values are calculated relative to the AD 1950 value of 427 $W \cdot m^{-2}$.

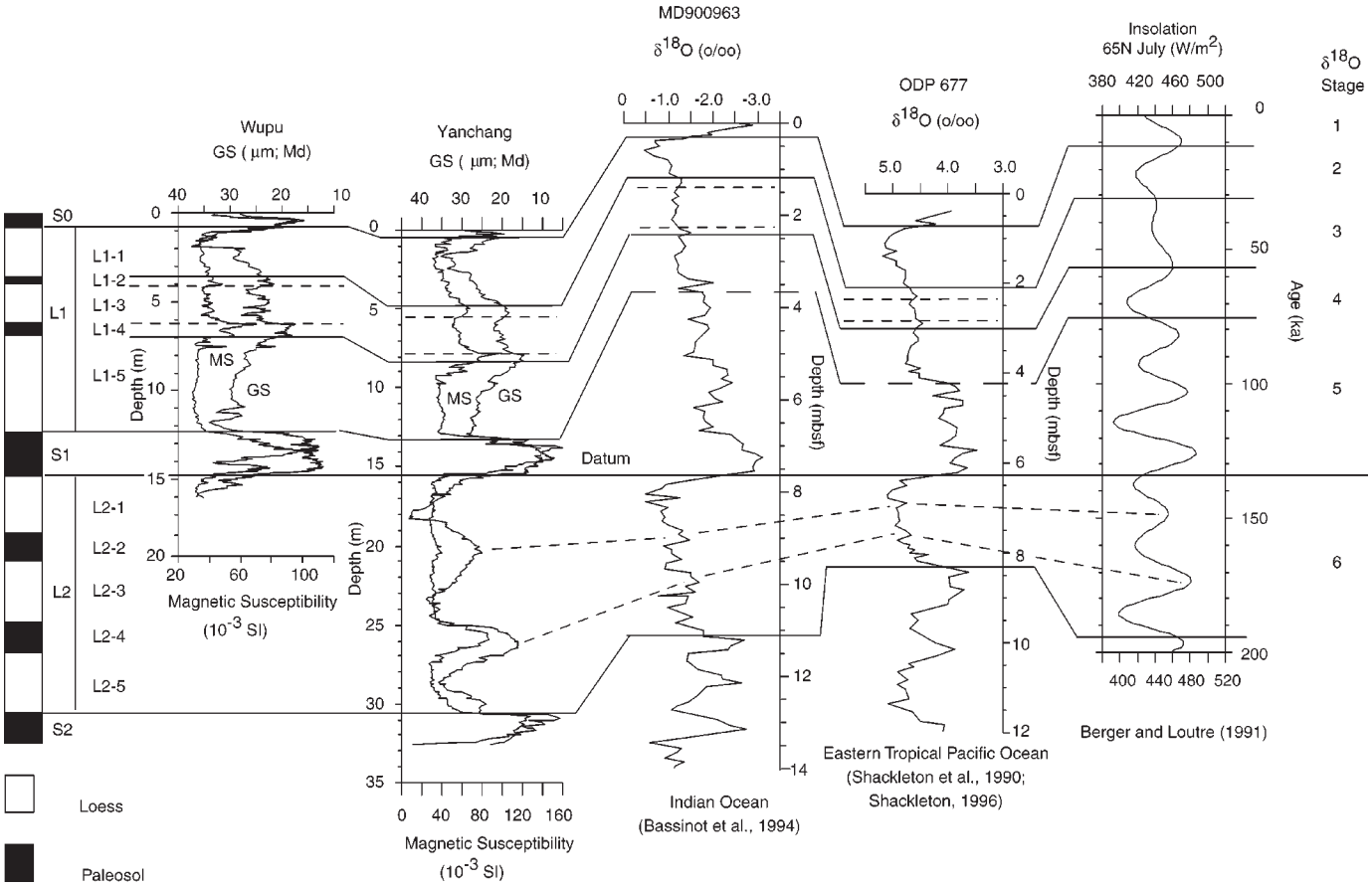

employed to identify interstadials (IS), and cold periods (C; e.g., stadials) within the last interglacial–glacial cycle.

At Wupu the last interglacial–glacial contact (S1–L1) is marked by a distinct increase in grain-size reflecting a change from a lower to higher wind strength toward the last glaciation (Rutter et al. 1995, 1997). Immediately above the S1–L1 contact are two peaks in grain-size (Fig. 11), alternating with two periods of decreased grain-size reflecting lower wind strength during relatively warm periods. The equivalent interval at Yanchang is more subdued because Yanchang is about 100 km downwind of Wupu. Similar observations of the presence of these warm–cold alternations have been made in the Loess Plateau by Porter and An (1995, Luochuan), Chen at al. (1997, Linxia), and Rutter et al. (1997, Ding Bien). Hence the warm and cold oscillations that mark the beginning of the last glaciation (MIS 2–4) are regionally consistent in the Loess Plateau.

In the Greenland record the last interglacial–glacial contact occurs at the base of a cold period (C20) in the $\delta^{18}O$ record. Similar to the loess records, two cold (C20, C19) and warm (IS20, IS19) oscillations, each lasting a few thousand years (Fig. 11), mark the beginning of the last glaciation. However, matching the base of cold period C20 to the MIS 5–4 boundary may be controversial in other environments. McManus et al. (1994) correlate high-resolution records of foraminiferal assemblages and ice-rafted detritus (IRD) from two North Atlantic cores (V29-191 and DSDP 609) with the GRIP ice-core (Dansgaard et al. 1993) and clearly place the last interglacial–glacial boundary at the top of IS 19. The cold periods, C19 and C20, appear as very subdued responses in the oceanic data sets, and are interpreted to have occurred during the last interglacial.

In addition, Kukla et al. (1997) correlate IRD, $\delta^{18}O$, and benthic foraminiferal records from V29-191 to the Grande Pile pollen record and again place the last interglacial–glacial boundary (MIS 5–4) at the top of IS 19 (a.k.a. W19 in Kukla et al. 1997). Relative to the Grande Pile record, the last interglacial–glacial boundary is placed about 30–40 cm above the base of a stadial that is marked by an increase in steppe vegetation (Kukla et al. 1997). In our loess records the interglacial–glacial boundary appears to correlate to the top of the St Germaine II interstadial, about 80–90 cm (using the Grande Pile depth scale) below the MIS 5–4 boundary defined by Kukla et al. (1997). Similar to the McManus (1994) reconstruction, Kukla et al. (1997) place the MIS 5–4 contact at the top of IS 19 because of the marked increase in *Neogloboquadrina pachyderma sinstral* above this level, and the subdued response of the aforementioned two cold periods in the V29-191 $\delta^{18}O$ data. There is clearly some difficulty in correlating the MIS 5–4 boundary between tropical marine and mid-latitude terrestrial records and, perhaps not surprisingly, our terrestrial records seem to concur with the Grande Pile and GISP2 $\delta^{18}O$ data.

Within MIS 4, the general increase in $\delta^{18}O$ in the GISP2 record reflects climatic warming, while the Chinese profiles show a decrease in grain-size reflecting lower wind strength.

The warming culminates in paleosol L1–4 in China and IS 14 in the GISP2 data (Grootes et al. 1993). Both L1–4 and IS 14 are responding to a summer insolation maximum identified by Berger and Loutre (1991) at about 56 ka. From the top of L1–4 a steady increase in grain-size occurs to about the top of L1–1 (MIS 2). The latter trend is marked by distinct variability in GS (especially at Wupu) in L1–3, which has a reasonably close correspondence to variations in the Greenland core. The base of MIS 2 is identified in our loess records by a weakly developed paleosol (L1–2). Our correlation between China and the GISP2 core equates L1–2 to IS 8, a correlation that is consistent with the other comparisons (Porter and An 1995; Chen et al. 1997; Rutter et al. 1997). However, the climostratigraphic correlation of L1–2 to IS 8 may be chronstratigraphically problematic. The midpoint of the warm period in the GISP2 and GRIP ice cores (about 37 ka and 34 ka, respectively; see Fig. 11; and see also Fig. 3 in Bond and Lotti 1995) precedes the insolation maximum identified by Berger and Loutre (1991) at 33 ka.

Comparing high-resolution loess records from China and the Indian and Pacific Oceans

Having established a reasonably reliable correlation to GISP2, we take a similar approach to correlating from China to the deep sea records, in that we search for warm periods within the glacials (e.g., L1–2 and L1–4, and IS 8 and IS 14, respectively) that are reasonably well expressed due to a relatively long time span and (or) magnitude of the warming. Grain-size and susceptibility profiles at Wupu and Yanchang are compared to $\delta^{18}O$ records from the Maldives Ridge (core MD900963; latitude 05°03.30′N; longitude 73°52.60′E) of the tropical Indian Ocean (Bassinot et al. 1994), and ODP 677 in the eastern equatorial Pacific Ocean (Shackleton et al. 1990; Shackleton 1996; ~latitude 1°12′N, longitude 83°44′E). Ocean core samples were taken approximately every 10 cm in ODP 677, and MD900963, resulting in a resolution of about 2 ka per sample.

In Fig. 12 we correlate using depth scales at each location (excluding the insolation record) to avoid the influence of age models that assume linear sedimentation rates. The assumption of linear sedimentation rates in high-resolution (i.e., a few thousand years per sample) terrestrial records is tenuous. For example, in the Loess Plateau sedimentation rates are higher during cold periods than warmer periods (Rutter et al. 1995). A brief examination of the thickness and time spans of the last two glacials and the last interglacial in oceanic records (all of which have nearly the same time span of about 60 ka; see Martinson et al. 1987) shows that the assumption of linear sedimentation rates is also tenuous, but perhaps less so than in terrestrial records.

In the loess records, the pedostratigraphy of L2 is similar to L1, in that L2 consists of three loess strata intercalated with two paleosols. The lower paleosols within L1 and L2 (L1–4 and L2–4) exhibit relatively better developed pedogenic features than the upper paleosols (L1–2 and L2–2) based on field observations. Similarly, the Berger and Loutre (1991) record identifies more intense insolation during the development of the lower soils. In addition, the ocean records consistently display lower ice volumes during the time of stronger pedogenic development (L2–4 and L1–4). Therefore, within the last two glaciations the relationship between insolation intensity, ice volume variations, and pedogenic development is quite consistent. Periods of maximum intensity correspond to minimums in ice volume and stronger paleosol development. We will now examine if this relationship is consistent during cold periods of the last two glaciations.

Within L2 the peak grain size in the three loess beds coarsens upward to a maximum in L2–1. Similarly, the ocean $\delta^{18}O$ records display increasing ice volumes to the top of MIS 6. The insolation profile displays three periods of minimum intensity during MIS 6 (185 ka, 160 ka, and 137 ka) corresponding to the three periods of increased grain-size and increased ice volumes in the loess and ocean records, respectively. However, the insolation profile shows that the lowest intensity occurs at about 185 ka near the base of MIS 6, while grain size and ice volume are highest near the top of MIS 6. This situation also occurs during the last glaciation (L1 = MIS 2–4). The ocean and loess records show that ice volume and grain size, respectively, are higher during MIS 2 (L1–1) than stage 4 (L1–5). However, insolation intensity is lower during MIS 4 than MIS 2. Hence, during the last two glaciations (MIS 6 and MIS 2–4) the minimums in insolation intensity to do not correspond linearly to periods of maximum grain-size and ice volume variations.

The last interglacial–glacial boundary (MIS 5–4) is difficult to determine in the ocean records. The key concept is to determine the presence of IS 19 and IS 20. We have suggested correlations, but recognize that the indetermination is problematic given the lower resolution of the available ocean data. Prell et al. (1986) used a graphical correlation method on ocean records to determine isotopic events that may be consistently recognized on a global scale. Similar to our method the authors correlated in the depth domain rather than the time domain. Within MIS 3, Prell et al. (1986) noticed the presence of warm periods (MIS 3.1 and 3.3) that we suggest correspond to L1–2 and L1–4 (and IS 8 and IS 14), respectively, in the terrestrial records. This correlation represents a consistent determination of high-resolution climate events between ocean, terrestrial, and ice-core environments.

Conclusions

We have compared and contrasted terrestrial and ocean proxy data over two different scales of resolutions to further our understanding of global climate history. Examining the records at two different resolutions allows us to focus on comparing Milankovitch and sub-Milankovitch climate forcing mechanisms in both environments. We have constructed our research in such a manner as to highlight the areas of accord and discord in the records. Specifically, our conclusions are as follows.

The close correspondence of the variations in the carbonate and mineral fractions in Hole 810C and core V21-146 suggest that the records reflect a regional influence in atmospheric and oceanic processes. The sediment mass accumulation rates (MAR) from Hole 810C and core V21-146 match very well throughout the last 500 ka, corroborating the potential of mass accumulation rates as a signal of

source area aridity. Volcanic ash skews the mineral grain-size results and makes interpretations of relative wind strength from Asian source areas more difficult. However, the ash beds hold significant promise as regional stratigraphic markers, and indicators of wind direction and strength, independent of continental aridity assumptions.

Proxy climate records that represent regional deposition from China and the western Pacific Ocean are then compared to determine the presence of Milankovitch-type periodicities. We believe that this is the first time that a wavelet analysis has been performed on multiple (and similar) records of proxy data from marine and terrestrial environments. The comparison of terrestrial and marine grain-size and magnetic susceptibility records indicate that dominant periods in one record may not be significant in another. Additionally, periods that are dominant in one record, may be dominant in another record at a different time. These factors point to the complexity of the deposition environments and to differences in the physical mechanisms through which deposition occurs in marine and terrestrial environment.

In the high-resolution records, we use depth scales, set within a temporal framework, to determine consistent, high-resolution climate boundaries. Correlations are made between a relatively high-latitude cryospheric environment to a mid-latitude terrestrial environment to a low-latitude oceanic environment. Our comparison certainly attests to the difficulty in determining globally consistent high-resolution climate boundaries in diverse environments.

The base of the last glaciation (L1) in the loess records corresponds to the base of a cold period (C20) in the Greenland GISP2 $\delta^{18}O$ record, and to the top of the St Germaine II interstadial in the Grande Pile pollen data. In the tropical ocean $\delta^{18}O$ data (e.g., V29-191) cold periods C20 and C19 are low amplitude responses relative to the other environments. Paleosols L1–4 and L1–2 in China correspond to warm periods IS 14 and 8 in the Greenland ice core, and to OIS 3.3 and 3.1 in the ocean core respectively, and form the basis for consistently determining the lower and upper boundaries of OIS 3.

Within the last two glaciations (MIS 6 and MIS 2–4) the periods of minimum insolation intensity do not correspond linearly to periods of maximum grain-size and ice volume variations in the loess and ocean records, respectively. However, during the warm interstadials of the last two glaciations, peaks in insolation intensity compare favourably with the times of strongest pedogenic development and minimum ice volume.

Acknowledgments

This paper is a contribution of the Canadian Climate System History and Dynamics Program supported by funding from the Natural Sciences and Engineering Research Council of Canada and the Atmospheric and Environment Service.

References

Bassinot, F.C., Labeyrie, L.D., Vincent, E., Quidelleur, X., Shackleton, N.J., and Lancelot, Y. 1994. The astronomical theory of climate and the age of the Brunhes-Matuyama magnetic reversal. Earth and Planetary Science Letters, **126**: 91–108.

Berger, A., and Loutre, M.F. 1991. Insolation values for the climate of the last 10 million years. Quaternary Science Reviews, **10**: 297–317.

Bond, G. and Lotti, R. 1995. Iceberg discharges into the North Atlantic on millennial time scales during the last glaciation. Science, **267**: 1005–1010.

Chao, S.-Y. 1994. Zonal jets over topography on a beta-plane, with applications to the Kuroshio Extension over Shatsky Rise. Journal of Physical Oceanography, **24**: 1512–1531.

Chen F.H, Bloemendal, J., Wang, J.M. Li, J.J., and Oldfield, F. 1997. High-resolution multi-proxy climate records from Chinese loess: Evidence for rapid climate changes over the last 75 kyr. Palaeogeography, Palaeoclimatology, Palaeoecology, **130**: 323–335.

Clemens, S.C., and Prell, W.L. 1990. Late Pleistocene variability of Arabian Sea summer monsoon winds and continental aridity: Eolian records from the lithogenic component of deep-sea sediments. Paleoceanography, **5**: 109–145.

Coulter, Inc. 1992. Coulter LS Series Reference Manual. Coulter Corporate Communications (#PN 4235896C), Hialeah, Fla.

Dansgaard, W., Johnsen, S., Clausen, H.B., Dahl-Jensen, D., Gundestrup, N., S., Hammer, C.U., Steffensen, J.P., Sveinbjornsdottir, A., Jouzel, J., and Bond, G. 1993. Evidence for general instability of past climate from a 250-kyr ice-core record. Nature, **364**: 218–220.

Ding, Z., Rutter, N.W., Liu, T.S., Evans, M.E., Yuchun, W. 1991. Climatic correlation between Chinese Loess and deep-sea cores: A structural approach. *In* Loess, environment and global Change. *Edited by* T.S. Liu. Science Press, Beijing, pp. 168–186.

Emiliani, C. 1955. Pleistocene temperatures. Journal of Geology, **63**: 538–578.

Farrell, J.W., and Prell, W.L. 1991. Pacific CaC03 preservation and $\delta^{18}0$ since 4 Ma: Paleoceanographic and paleoclimatic implications. Paleoceanography, **6**: 485–498.

Folk, R.L. 1974. Petrology of sedimentary rocks. Hemphill, Austin, Tex.

Furuta, T., Fujioka, K., and Arai, F. 1986. Widespread submarine tephras around Japan-Petrographic and chemical properties. Marine Geology, **72**: 125–142.

Grootes, P.M., Stuiver, M., White, J.W.C., Johnsen, S., and Jouzel, J. 1993. Comparison of oxygen isotope records from the GISP2 and GRIP Greenland ice-cores. Nature, **366**: 552–554.

Haug, G.H., Maslin, M.A., Sarnthein, M., Stax, R., and Tiedemann, R. 1995. Evolution of Northwest Pacific sedimentation patterns since 6 Ma (Site 882). *In* Proceedings of the Ocean Drilling Program, Scientific Results, 145. *Edited by* D.K. Rea, I.A. Basov, D.W. Scholl, and J.F. Allan. Ocean Drilling Program, College Station, Tex., pp. 293–314.

Hovan, S.A., Rea, D.K., Pisias, N.G., and Shackleton, N.J. 1989. A direct link between the China loess and marine $\delta^{18}0$ records: aeolian flux to the north Pacific. Nature, **340**:296–298.

Hovan, S.A., Rea, D.K., and Pisias, N.G. 1991. Late Pleistocene continental climate and oceanic variability recorded in northwest Pacific sediments. Paleoceanography, **6**: 349–370.

Hurlburt, H.E., Wallcraft, A.J., Schmitz, W.J., Jr., Hogan, P.J., and Metzger, E.J. 1996. Dynamics of the Kuroshio/Oyashio current system using eddy-resolving models of the North Pacific Ocean. Journal of Geophysical Research, **101**: 941–976.

Imbrie, J., Hays, J.D., Martinson, D.G., McIntyre, A., Mix, A.C., Morley, J.J., Pisias, N.G., Prell, W.L., and Shackleton, N.J. 1984. The orbital theory of Pleistocene climate: Support from a revised chronology of the marine $\delta^{18}0$ record. *In* Milankovitch and Climate, Part 1. *Edited by* A. Berger, J. Imbrie, J. Hays, G.

Kukla, and B. Saltzman. D. Reidel Publishing Company. pp. 269–305.

Jacobi, R.D., and Hayes, D.E. 1989. Sedimentary effects of the interplay between the Kuroshio Extension and Pacific plate motion. Geological Society of America Bulletin, **101**: 549–560.

Jacobsen, G.L., Jr., Webb, T., III, and Grimm, E.C. 1987. Patterns and rates of vegetation change during the deglaciation of eastern North America. *In* North America and adjacent oceans during the last deglaciation. *Edited by* W.F. Ruddiman and Wright, H.E., Jr. Geological Society of America, The geology of North America, Vol. K-3.

Janecek, T.J., and Rea, D.K. 1983. Eolian deposition in the northeast Pacific Ocean: Cenozoic history of atmospheric circulation. Geological Society of America Bulletin, **94**: 730–738.

Janecek, T.J., and Rea, D.K. 1985. Quaternary fluctuations in Northern Hemisphere tradewinds and westerlies. Quaternary Research, **24**: 150–163.

Johnsen, S.J., Clausen, H.B., Dansgaard, W., Fuhrer, K., Gundestrup, N., Hammer, C.U., Iversen, P., Jouzel, J., Stauffer, B., and Steffensen, J.P. 1992. Irregular glacial interstadials recorded in a new Greenland ice-core. Nature, **359**: 311–313.

Joyce, T.M. 1987. Hydrographic sections across the Kuroshio Extension at 165°E and 175°W. Deep Sea Research, **34**: 1331–1352.

Koblinsky, C.J., Niiler, P.P., and Schmitz, W.J., Jr. 1989. Observations of wind-forced deep ocean currents in the North Pacific. Journal of Geophysical Research, **94**: 10 773–10 790.

Konert, M., and Vandenberghe, J. 1997. Comparison of laser grain-size analysis with pipette and sieve analysis: a solution for the underestimation of the clay fraction. Sedimentology, **44**: 523–535.

Krissek, L.A. 1995. Late Cenozoic ice-rafting records from Leg 145 sites in the North Pacific: Late Miocene onset, Late Pliocene intensification, and Pliocene-Pleistocene events. *In* Proceedings of the Ocean Drilling Program, Scientific Results, 145. *Edited by* D.K. Rea, I.A. Basov, D.W. Scholl, and J.F. Allan. Ocean Drilling Program, College Station, Tex., pp. 179–194.

Krissek, L.A., Morley, J.J., and Lofland, D.K. 1985. The occurrence, abundance, and composition of ice-rafted debris in sediments from Deep Sea Drilling Project sites 579 and 580, Northwest Pacific. *In* Initial Reports, Deep Sea Drilling Project, 86. *Edited by* G.R. Heath, L.H. Burckle, et al.. Ocean Drilling Program, College Station, Tex., pp. 647–655.

Kukla, G. 1987. Loess stratigraphy in central China. Quaternary Science Review, **6**: 191–219.

Kukla, G., An, Z.S., Melice, J.L., Gavin, J., and Xia, J.L. 1990. Magnetic susceptibility record of Chinese loess. Transactions of the Royal Society of Edinburgh: Earth Sciences, **81**: 263–288.

Kukla, G., McManus, J. F., Rousseau, D.D., and Chuine, I. 1997. How long and how stable was the last interglacial? Quaternary Science Reviews, **16**: 605–612.

Leinen, M., and Heath, G.R. 1981. Sedimentary indicators of atmospheric activity in the Northern Hemisphere during the Cenozoic. Palaeogeography, Palaeoclimatology, Palaeoecology, **36**: 1–21.

Liu et al. 1985. Loess and the environment. Science Press, Beijing.

Machida, H., and Arai, F. 1976. The widespread tephra—The Aira-Tn ash. Kagaku, **46**: 339–347.

Machida, H., and Arai, F. 1978. Akahoya ash — A widespread tephra erupted from the Kikai caldera, southern Kyushu, Japan. Quaternary Research of Japan, **17**: 143–163.

Machida, H., and Arai, F. 1983. Extensive ash falls in and around the sea of Japan from large Late Quaternary eruptions. Journal of Volcanology and Geothermal Research, **18**: 151–164.

Machida, H., and Arai, F. 1988. A review of Late Quaternary deep-sea tephras around Japan. Quaternary Research of Japan, **26**: 227–242.

Martinson, D.G., Pisias, N.G., Hays, J.D., Imbrie, J., Moore, T.C., Jr., and Shackleton, N.J. 1987. Age dating and the orbital theory of the ice ages; development of a high-resolution 0 to 300 000-year chronostratigraphy. Quaternary Research, **27**: 1–29.

McCave, L.N., and Syvitski, J.P.M. 1991. Principles and methods of geological particle size analysis. *In* Principles, Methods and application of particle size analysis. *Edited by* J.P.M. Syvitski. Cambridge University Press, New York, pp. 3–21.

McCave, L.N., Manighetti, B., and Robinson, S.G. 1995. Sortable silt and fine sediment size/composition slicing: Parameters for paleocurrent speed and paleoceanography. Paleoceanography, **10**: 593–610.

McManus, J.F., Bond, G.C., Broecker, W.S., Johnsen, S., Labeyrie, L., and Higgins, S., 1994. High-resolution climate records from the North Atlantic during the last interglacial. Nature **371**: 326–329.

Meese, D., Alley, R., Gow, T., Grootes, P.M., Mayewski, P., Ram, M., Taylor, K., Waddington, E., and Zielinski, G. 1994. Preliminary depth-age scale of the GISP2 ice-core. United States Army Corps of Engineers, Cold Regions Research and Engineering Laboratory, Special Report 94–1.

Nakai, S., Halliday, A.N., and Rea, D.K. 1993. Provenance of dust in the Pacific Ocean. Earth and Planetary Science Letters, **119**: 143–157.

Natland, J.H. 1993. Volcanic ash and pumice at Shatsky Rise: Sources, mechanisms of transport, and bearing on atmospheric circulation. *In* Proceedings of the Ocean Drilling Program, Scientific Results, 132. *Edited by* J.H. Natland and M. Storms. Ocean Drilling Program, College Station, Tex., pp. 57–66.

North American Stratigraphic Code. 1983. American Association of Petroleum Geologists Bulletin, **67**: 841–875.

Olivarez, A.M., Owen, R.M., and Rea, D.K. 1991. Geochemistry of eolian dust in Pacific pelagic sediments: Implications for paleoclimatic interpretations. Geochimica et Cosmochimica Acta, **55**: 2147–2158.

Porter, S.C., and An, Z.S. 1995. Correlation between climate events in the North Atlantic and China during the last glaciation. Nature, **375**: 305–308.

Prell, W.L., Imbrie, J., Martinson, D.G., Morley, J.J., Pisias, N.G., Shackleton, N.J., and Streeter, H. 1986. Graphic correlation of oxygen isotope stratigraphy application to the late Quaternary. Paleoceanography, **1**: 137–162.

Premoli Silva, I., Castradori, D., and Spezzaferri, S. 1993. Calcareous nannofossil and planktonic foraminifer biostratigraphy of Hole 810C (Shatsky Rise, Northwestern Pacific). *In* Proceedings of the Ocean Drilling Program, Scientific Results, 132. *Edited by* J.H. Natland and M. Storms. Ocean Drilling Program, College Station, Tex., pp. 15–36.

Rack, F.R., Janecek, T.R., Swart, P.K., and Brass, G.W. 1993. Data Report: High resolution carbonate and oxygen isotope data from Site 810: Comparison to GRAPE bulk density and magnetic susceptibility data. *In* Proceedings of the Ocean Drilling Program, Scientific Results, 132. *Edited by* J.H. Natland and M. Storms. Ocean Drilling Program, College Station, Tex., pp. 69–79.

Rack, F.R., Janecek, T.R., Erba, E., Fenner, J., and Gee, J.S. 1995. Synthesis of terrigenous accumulation rates and biostratigraphic studies at sites in the northwestern Pacific Ocean, with comparisons to adjacent regions of the Pacific Gyre. *In* Proceedings of the Ocean Drilling Program, Scientific Results, 144. *Edited by* J.A. Haggerty, I. Premoli Silva, F.R. Rack, and M.K. McNutt. Ocean Drilling Program, College Station, Tex., pp. 691–736.

Raffi, I., and Flores, J.-A. 1995. Pleistocene through Miocene calcareous nannofossils from eastern equatorial Pacific Ocean (ODP Leg 138). *In* Proceedings of the Ocean Drilling Program,

Scientific Results, 138. *Edited by* N. Pisias, L.A. Mayer, T.R. Janecek, et al.. Ocean Drilling Program, College Station, Tex., pp.223–286.

Raffi, I., Backman, J., Rio, D., and Shackleton, N.J. 1993. Plio-Pleistocene nannofossil biostratigraphy and calibration to oxygen isotope stratigraphies from Deep Sea Drilling Project Sit 607 and Ocean Drilling Program Site 677. Paleoceanography, **8**: 387 408.

Rea, D.K. 1994. The paleoclimatic record provided by eolian deposition in the deep sea: The geologic history of wind. Reviews of Geophysics, **32**: 159–195.

Rea, D.K., and Hovan, S.A. 1995. Grain-size distribution and depositional processes of the mineral component of abyssal sediments: lessons from the North Pacific. Paleoceanography, **10**: 251–258.

Rea, D.K., and Janecek, T.R. 1981. Mass accumulation rates of non-authigenic inorganic crystalline (eolian) components of deep sea sediments from the western Mid-Pacific Mountains, Deep Sea Drilling Project Site 463. *In* Initial Reports, Deep Sea Drilling Project 62. *Edited by* L.N. Stout, J. Thiede, T.L. Vallier et al. Ocean Drilling Program, College Station, Tex., pp. 653–659.

Rea, D.K., and Janecek, T.R. 1982. Late Cenozoic changes in atmospheric circulation deduced from North Pacific eolian sediments. Marine Geology, **49**: 149–167.

Rea, D.K., Leinen, M., and Janecek, T.R. 1985. Geologic approach to the long-term history of atmospheric circulation. Science, **227**: 721–725.

Rutter, N.W., Ding, Z., and Liu, T. 1995. Reliability of grain-size variation as a climatic proxy and correlation method for loess-paleosol units, North-Central China. *In* Proceedings of Conference on Geology, Geotechnology, and Mineral Resources of Indochina (GEO-INDO'95): 45–52.

Rutter, N.W., Rokosh, D., Ding, Z., Ren, J., Sun, J., and Liu, T. 1997. High resolution paleoclimate records from the Loess Plateau and desert margins, North-Central China. Palaeoecology of Africa, **25**: 321–241.

Sager, W.W., Polgreen, E.L., and Rack, F.R. 1993. Magnetic polarity reversal stratigraphy of Hole 810C, Shatsky Rise, Western Pacific Ocean. *In* Proceedings of the Ocean Drilling Program, Scientific Results, 132. *Edited by* J.H. Natland and M. Storms. Ocean Drilling Program, College Station, Tex., pp. 47–55.

Schmitz, W.J., Jr., Niiler, P., and Koblinsky, C.J. 1987. Two-year moored instrument results along 152°E. Journal of Geophysical Research, **92**: 10 826–10 834.

Shackleton, N. 1996. Timescale Calibration, ODP 677. IGBP PAGES/World Data Center—A for Paleoclimatology Data Contribution Series #96–018. NOAA/NGDC Paleoclimatology Program, Boulder, Colo.

Shackleton, N.J., Berger, A., and Peltier, W.R. 1990. An alternative astronomical calibration of the lower Pleistocene timescale based on ODP Site 677. Transactions of the Royal Society of Edinburgh, Earth Sciences, **81**: 251–261.

Shackleton, N.J., Crowhurst, S., Hagelberg, T., Pisias, N.G., and Schneider, D.A. 1995. A new Late Neogene time scale: Application to Leg 138 sites. *In* Proceedings of the Ocean Drilling Program, Scientific Results, 138. *Edited by* N. Pisias, L.A. Mayer et al.. Ocean Drilling Program, College Station, Tex., pp. 73–101.

Storms, M.A., Natland, J.H., Rack, F.R. et al. (Editors.) 1991. Proceedings of the Ocean Drilling Program, Ocean Drilling Program, College Station, Tex. Initial Reports, 132.

Stuiver, M., Grootes, P., and Braziunas, T.F. 1995. The GISP2 18O climate record of the past 16,500 years and the role of the sun, ocean, and volcanoes. Quaternary Research, **44**: 341–354.

Sun, J., and Ding, Z.1998. Deposits and soils of the past 130 000 years at the desert-loess transition in northern China. Quaternary Research, **50**,2, 148–156.

Weber, E.T., Owen, R.M., Dickens, G.R., Halliday, A.N., Jones, C.E., and Rea, D.K. 1996. Quantitative resolution of eolian continental crustal material and volcanic detritus in North Pacific surface sediment. Paleoceanography, **11**: 115–127.